**Steel and Composite Structures**, *Vol. 29, No. 1 (2018) 91-106*
DOI: https://doi.org/10.12989/scs.2018.29.1.091


# Theoretical and experimental study on deflection of steel-concrete composite truss beams

Junli Wang [1], Tian Li [1] and Lisheng Luo [*2]

[1] *School of Civil Engineering, Zhengzhou University, Zhengzhou 450001, China*
[2] *College of Civil Engineering and Architecture, Hainan University, Haikou 570228, China*

(*Received April 14, 2018, Revised July 21, 2018, Accepted July 31, 2018*)

**Abstract.** This paper investigates the deflection of the steel-concrete composite truss beam (SCCTB) at the serviceability limit state. A precise solution for the distributed uplift force of the SCCTB, considering five different loading types, is first derived based on the differential and equilibrium equations. Furthermore, its approximate solution is proposed for practical applications. Subsequently, the shear slip effect corresponding to the shear stiffness of the stub connectors, uplift effect corresponding to the axial stiffness of the stub connectors and shear effect corresponding to the brace deformation of the steel truss are considered in the derivation of deflection. Formulae for estimating the SCCTB deflection are proposed. Moreover, based on the proposed formulae, a practical design method is developed to provide an effective and convenient tool for designers to estimate the SCCTB deflection. Flexure tests are carried out on three SCCTBs. It is observed that the SCCTB stiffness and ultimate load increase with an increase in the shear interaction factor. Finally, the reliability of the practical design method is accurately verified based on the available experimental results.

**Keywords:** serviceability limit state; uplift effect; deflection; steel-concrete composite truss beam; flexural tests

## 1. Introduction

With the development in construction techniques of building structures, increasingly innovative large-span bridges, large-span spatial structures (Xiong *et al*. 2017) and super high-rise structures (Luo *et al*. 2015) have appeared. In order to satisfy the economy and security requirements of these structures, steel-concrete composite members have been proposed. Steel-concrete composite members can appropriately utilise the material properties of the steel and concrete (Xian *et al*. 2017, Xiong *et al*. 2016). Therefore, numerous steel-concrete composite joints (Jiang *et al*. 2017), columns (Huang *et al*. 2016, Zhang *et al*. 2018), beams (Ding *et al*. 2018) and shear walls (Elmatzoglou and Avdelas 2017) have been designed. As an important component of composite structures, the steel-concrete composite beam has become increasingly popular, with a large number of studies having reported on its flexural behaviour (Pathirana *et al*. 2016, Liu *et al*. 2017), dynamic behaviour (Henderson *et al*. 2015), reinforcement methods (Subhani *et al*. 2018, El-Zohairy *et al*. 2017, Karam *et al*. 2017) and numerical simulation (Katwal *et al*. 2018, Lou *et al*. 2016, Goncalves 2018). Following the research on traditional steel-concrete composite beams, the innovative steel-concrete composite truss beam (SCCTB), which is commonly composed of a steel truss and concrete slab, has received significant attention in recent years. The SCCTB offers numerous advantages, such as steel savings, favourable load-bearing behaviour, and high space utilisation. As a result, the SCCTB has been applied extensively to large-span bridges, spatial structures and high-rise structures globally, including the Kleve-Emmerich Bridge (Germany), Tsing Ma Bridge (Hong Kong, China), Wuxi Grand Theatre (China) and Willis Tower (America).

The composite action of the SCCTB is achieved by connecting the steel truss and concrete slab with shear connectors. In fact, the shear connectors could be deformed with a finite stiffness, resulting in the development of interfacial shear slip between the steel truss and concrete slab (Liu *et al*. 2016). This interfacial shear slip may have a significant influence on the SCCTB mechanical behaviour. Therefore, progress has been made by various researchers in understanding the SCCTB connection behaviour. Yin *et al*. (2017) investigated the SCCTB connection behaviour for bridge applications by means of an experimental study and finite element analysis, and found that the connection exhibits an excellent load-bearing capacity, with sufficient safety factors and satisfactory ductility. According to experimental and numerical results, Machacek and Cudejko (2013) and Machacek and Charvat (2017) presented the longitudinal shear distribution along an interface between the steel and concrete parts of the SCCTB, from the elastic phase until plastic collapse, and observed that the nonlinear distribution of the longitudinal shear depends significantly on the rigidity of the shear connection and densification of the shear connectors above the truss nodes. Lai *et al*. (2017) developed a finite beam element method program for the SCCTB natural vibration frequency and indicated that shear deformation has an important effect on the SCCTB high-order natural vibration frequency. Jiang *et al*. (2018)

∗Corresponding author, Ph.D.,
E-mail: luolisheng2015@hainu.edu.cn



ISSN: 1229-9367 (Print), 1598-6233 (Online)

proposed an analytical method for calculating the SCCTB natural frequency, and found that the influence of the interface slip stiffness and shear deformation on the SCCTB natural frequency could not be neglected.

Hence, to obtain the precise deflection of the SCCTB, the partial shear interaction of the shear connectors should be considered. In recent years, numerous researchers have proposed various methods for calculating the deflection of the steel-concrete composite beam. Amadio *et al*. (2012) investigated the steel-concrete composite beam deflection using accurate finite element models, and proposed a simple design criterion that considers the serviceability limit state and connection flexibility. Taking into account the shear lag effect of the steel-concrete composite deck, Zhu *et al*. (2015) proposed prediction formulae for the effective width and applied a simplified analytical method of a composite continuous I-girder deck for the design process, based on a general beam element model. Based on higher-order beam theory, Wen *et al*. (2018) developed an exact analytical model for accurate prediction of the flexural response of two-layered composite beams with partial shear interactions. Song *et al*. (2018) reported on a residual deflection analysis in the negative moment regions of steel-concrete composite beams, and provided fatigue design recommendations. Uddin *et al*. (2018) presented a geometrically nonlinear inelastic analysis of steel-concrete composite beams with partial interaction using higher-order beam theory. However, available design methods for the SCCTB deflection are limited, resulting in significant obstruction of its application and development.

SCCTBs are generally used in engineering structures with larger span-to-height ratios. In order to satisfy the serviceability limit state, a practical design method for the SCCTB deflection is required. Studs belonging to the flexible shear connectors are used extensively in the SCCTB. Therefore, the shear slip effect corresponding to the shear stiffness and uplift effect corresponding to the axial stiffness of the stub connectors should be considered. Moreover, the shear effect of the steel truss may have a significant influence on the SCCTB deflection. This study investigated the influence of the shear slip, uplift and shear effects on the SCCTB deflection at the serviceability limit state. Considering these effects, practical formulae for estimating the SCCTB deflection under five different loading types were developed. Moreover, in order to verify the reliability of the proposed formulae, flexural tests were carried out on three SCCTB specimens.

## 2. Theoretical derivation of the uplift force

### *2.1 Basic assumptions*

The steel truss and concrete slab are two different composite parts of the SCCTB. As the SCCTB is loaded, a deflection difference and slip deformation appear between the steel truss and concrete slab, leading to the generation of a vertical uplift force and horizontal shear force. Numerous researchers have discussed the shear force (Wen *et al*. 2018). In this section, the formulae for estimating the uplift force are derived. Prior to providing the theoretical derivations, three basic assumptions are made, as follows.

(1) The force between the steel truss and concrete slab is fully transferred by the stud connectors. Therefore, the compressive force and friction of the interface between the steel truss and concrete slab are ignored.
(2) The stud connectors can be replaced by continuous elastic material. Thereby, the vertical uplift and horizontal shear forces are indirectly proportional to the deflection difference and slip deformation between the steel truss and concrete slab, respectively. Moreover, the concentrated uplift force is replaced by the distributed uplift force.
(3) For the serviceability limit state, the steel truss and concrete slab remain in the elastic phase. As a result, they assumed as two types of continuous elastic materials. When the SCCTB operates at the serviceability limit state, the steel truss and concrete slab obey the plane cross-section assumption and basic bending theory; however, their curvatures differ.

### *2.2 Theoretical formulae of the uplift force*

The uplift force of the simply supported SCCTB considering five different loading types was derived based on the differential and equilibrium equations. The five loading types included a concentrated load at the middle of the beam span $P_1$, two concentrated loads at the 1/3 beam span $P_2$, a uniformly distributed load $q$, a concentrated load at any position of the beam span $P_3$ and two concentrated loads at a symmetrical position of the beam span $P_4$, as illustrated in Fig. 1. A finite length $dx$ of the simply supported SCCTB, and its corresponding deformation and internal force, are plotted in Fig. 2, where $b_1$ is the distance

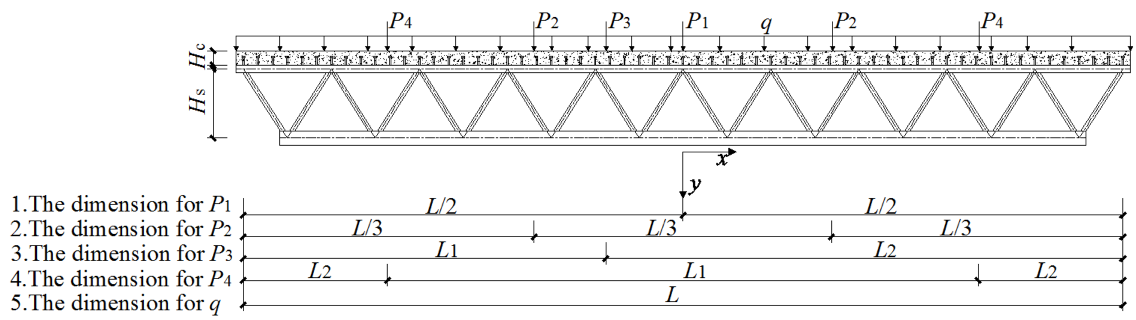


Fig. 1 Five different loading types

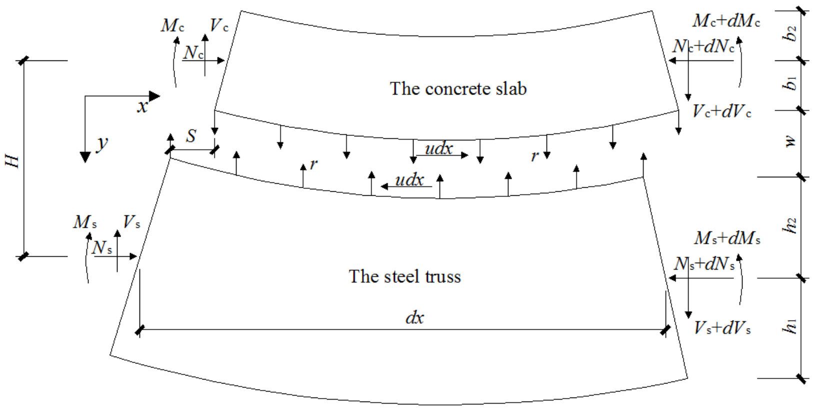


Fig. 2 Deformation and internal force of a finite length *dx*

from the centroidal axis to the concrete slab bottom; $b_2$ is the distance from the centroidal axis to the concrete slab top; $h_1$ is the distance from the centroidal axis to the steel truss top; $h_2$ is the distance from the centroidal axis to the steel truss bottom; $N_c$ is the axial force applied to the concrete slab; $N_s$ is the axial force applied to the steel truss; $M_c$ is the bending moment acting on the concrete slab; $M_s$ is the bending moment acting on the steel truss; $V_c$ is the shear force applied to the concrete slab; $V_s$ is the shear force applied to the steel truss; $r$ is the distributed uplift force applied to the continuous elastic material used to replace the stud connectors; $u$ is the distributed shear force applied to the continuous elastic material used to replace the stud connectors; $S$ is the slip deformation between the steel truss and concrete slab; and $w$ is the deflection difference between the steel truss and concrete slab.

### 2.2.1 A concentrated load at the middle of the beam span

The detailed derivation for the uplift force of the simply supported SCCTB subjected to a concentrated load at the middle of the beam span $P_1$ is expressed as follows.

Assumption (2) yields

$$R = pr = k_v(y_s - y_c) = k_v w \tag{1}$$

$$r = \frac{k_v}{p}(y_s - y_c) \tag{2}$$

where $R$ is the uplift force applied to a single stud connector; $p$ is the longitudinal spacing of the stud connectors; $k_v$ is the axial stiffness of the stub connectors; $y_s$ is the deflection of the steel truss; and $y_c$ is the deflection of the concrete slab.

The second derivative of Eq. (2) is

$$\frac{d^2r}{dx^2} = \frac{k_v}{p}\left(\frac{d^2y_s}{dx^2} - \frac{d^2y_c}{dx^2}\right) \tag{3}$$

According to the basic theory of the mechanics of materials, Eq. (3) can be transformed into Eq. (4).

$$\frac{d^2r}{dx^2} = \frac{k_v}{p}\left(\frac{M_c}{E_cI_c} - \frac{M_s}{E_sI_s}\right) \tag{4}$$

where $E_c$ is the elastic modulus of concrete; $I_c$ is the moment of inertia of the concrete slab cross-section with an effective width; $M_s$ is the bending moment acting on the steel truss; $E_s$ is the elastic modulus of steel; and $I_s$ is the moment of inertia of the steel truss cross-section.

Hence, the second derivative of Eq. (4) is

$$\frac{d^4r}{dx^4} = \frac{k_v}{p}\left(\frac{1}{E_cI_c}\frac{d^2M_c}{dx^2} - \frac{1}{E_sI_s}\frac{d^2M_s}{dx^2}\right) \tag{5}$$

Ignoring the higher-order derivative terms, the moment equilibrium equation for the left-section centroid of the concrete slab (Fig. 2) can be expressed as

$$V_c dx - udxb_1 = dM_c \tag{6}$$

Therefore, the first derivative of Eq. (6) is

$$\frac{d^2M_c}{dx^2} = \frac{dV_c}{dx} - b_1\frac{du}{dx} \tag{7}$$

Meanwhile, a similar derivation to that of Eq. (7) can be applied to Eq. (8),and the moment equilibrium equation for the left-section centroid of the steel truss (Fig. 2) can be expressed as

$$\frac{d^2M_s}{dx^2} = \frac{dV_s}{dx} - \frac{du}{dx}h_1 \tag{8}$$

According to the force equilibrium conditions of the concrete slab and steel truss, Eqs. (9) to (11) can be obtained.

$$r = -\frac{dV_c}{dx} \tag{9}$$

$$r = \frac{dV_s}{dx} \tag{10}$$

$$u = \frac{dN}{dx} \tag{11}$$

where $N = N_s = N_c$.

Combining Eq. (5) with Eqs. (7) to (11), Eq. (12) can be derived.

$$\frac{d^4r}{dx^4}+mr+n\frac{d^2N}{dx^2}=0 \tag{12}$$

where the expressions of $m$ and $n$ are provided in Appendix 1.

According to Eq. (12), in order to obtain the distributed uplift force $r$, the solution of the axial force $N$(x) should first be derived. Assumption (2) yields

$$Q=pu=k_lS \tag{13}$$

where $Q$ is the shear force applied to a single stud connector and $k_l$ is the shear stiffness of the stub connectors.

Hence, the derivative of Eq. (13) is

$$\frac{du}{dx}=\frac{k_l}{p}\frac{dS}{dx} \tag{14}$$

Based on the deformation compatibility condition of the steel truss and concrete slab, Eq. (15) is obtained

$$\Delta\varepsilon=dS/dx=\varepsilon_s-\varepsilon_c \tag{15}$$

Combining Eq. (14) with Eqs. (11) and (15), Eq. (16) is obtained

$$\frac{d^2N}{dx^2}=\frac{k_l}{p}(\varepsilon_s-\varepsilon_c) \tag{16}$$

According to the basic theory of the mechanics of materials, Eq. (16) can be transformed into Eq. (17).

$$\frac{d^2N}{dx^2}=\frac{k_l}{p}(\frac{1}{E_cA_c}+\frac{1}{E_sA_s})N-\frac{k_l}{p}(\frac{M_s}{E_sI_s}h_1+\frac{M_c}{E_cI_c}b_1) \tag{17}$$

According to the bending moment equilibrium condition of the SCCTB, Eq. (18) can be obtained

$$M_s+M_c=M-NH \tag{18}$$

where $M$ is the external bending moment applied to the SCCTB and $H$ is the distance from the centroid of the steel truss cross-section to the centroid of the concrete slab cross-section, as illustrated in Fig. 2.

Combining Eq. (18) with Eq. (4), Eqs. (19) and (20) can be derived.

$$\frac{M_c}{E_cI_c}=\frac{E_sI_sp}{(E_cI_c+E_sI_s)k_v}\frac{d^2r}{dx^2}+\frac{M-NH}{E_cI_c+E_sI_s} \tag{19}$$

$$\frac{M_s}{E_sI_s}=-\frac{E_cI_cp}{(E_cI_c+E_sI_s)k_v}\frac{d^2r}{dx^2}+\frac{M-NH}{E_cI_c+E_sI_s} \tag{20}$$

Hence, combining Eq. (17) with Eqs. (19) and (20), Eq. (21) is obtained

$$\frac{d^2N}{dx^2}=aN-f\frac{d^2r}{dx^2}-gM \tag{21}$$

where the expressions of $a$, $f$ and $g$ are provided in Appendix 1.

By combining Eq. (12) with Eq. (21) and $d^2M/dx^2=0$, the differential equation for the distributed uplift force $r$ is derived in Eq. (22)

$$\frac{d^6r}{dx^6}-A\frac{d^4r}{dx^4}+B\frac{d^2r}{dx^2}-Cr=0 \tag{22}$$

where the expressions of $A$, $B$ and $C$ are provided in Appendix 1.

According to the differential equation in Eq. (22), the solution for the distributed uplift force $r$ can be derived, as expressed in Eq. (23).

$$\begin{aligned}r(x)&=C_1e^{\lambda_1x}+C_2e^{-\lambda_1x}+(C_3\cos\beta x+C_4\sin\beta x)e^{\alpha x}\\&+(C_5\cos\beta x+C_6\sin\beta x)e^{-\alpha x}\end{aligned} \tag{23}$$

where $C_i$ ($i$ = 1, 2, 3,…) represent the constants that can be determined by the boundary conditions; $\lambda_1$ is the real root of the characteristic equation; and $\alpha$ and $\beta$ are the real and imaginary parts of the complex root of the characteristic equation, respectively.

Eq. (23) is complex; for practical application, the approximate solution for the distributed uplift force is proposed. It is found that, when $f\to 0$, $f/a\to 0$ and $f/g\to 0$, and $d^2N/dx^2$ and $d^2r/dx^2$ are the same order of magnitude. Therefore, Eq. (21) is approximately equivalent to Eq. (24).

$$\frac{d^2N}{dx^2}=aN-gM \tag{24}$$

The axial force $N(x)$ comprises the general solution $N_1(x)$ and particular solution $N_2(x)$, and $N_1(x)$ is expressed as follows

$$N_1(x)=C_7e^{\sqrt{a}x}+C_8e^{-\sqrt{a}x} \tag{25}$$

The bending moment applied to the right-hand segment of the simply supported SCCTB is

$$M(x)=\frac{P_1}{2}(\frac{L}{2}-x) \tag{26}$$

Therefore, $N_2(x)$ is

$$N_2(x)=\frac{g}{a}M \tag{27}$$

The first boundary condition is that the axial force applied to the steel truss and concrete slab at the support position of the simply supported SCCTB is zero, as illustrated in Eq. (28). The second boundary condition is that the slip deformation between the steel truss and concrete slab at the middle of the simply supported SCCTB is zero owing to the symmetrical characteristic, as illustrated in Eq. (29). According to the boundary conditions, the constants $C_7$ and $C_8$ can be determined, as expressed in Appendix 2. Therefore, $N(x)$ is derived, as expressed in Eq. (30).

$$N\Big|_{x=\frac{L}{2}}=0,\ \frac{d^2N}{dx^2}\Big|_{x=\frac{L}{2}}=0 \tag{28}$$

$$\left.\frac{dN}{dx}\right|_{x=0}=0 \tag{29}$$

$$N(x)=\frac{P_1 g}{2a\sqrt{a}(1+e^{\sqrt{a}L})}e^{\sqrt{a}x}-\frac{P_1 g}{2a\sqrt{a}(1+e^{-\sqrt{a}L})}e^{-\sqrt{a}x}+\frac{g}{a}M \tag{30}$$

By combining Eq. (12) with Eq. (30), $r(x)$ can be obtained, as expressed in Eqs. (31) to (33). The axial force $r(x)$ comprises the particular solution $r_1(x)$ and general solution $r_2(x)$.

$$r(x)=r_1(x)+r_2(x) \tag{31}$$

$$r_1(x)=-\frac{na}{m+a^2}\left[\frac{P_1 g}{2a\sqrt{a}(1+e^{\sqrt{a}L})}e^{\sqrt{a}x}-\frac{P_1 g}{2a\sqrt{a}(1+e^{-\sqrt{a}L})}e^{-\sqrt{a}x}\right] \tag{32}$$

$$r_2(x)=(C_9\cos\beta x+C_{10}\sin\beta x)e^{\alpha x}+(C_{11}\cos\beta x+C_{12}\sin\beta x)e^{-\alpha x} \tag{33}$$

The third boundary condition is the equilibrium condition of the concrete slab under a vertical force, as expressed in Eq. (34).

$$\int_0^{L/2} r(x)dx=-\frac{P_1}{2} \tag{34}$$

According to the three aforementioned boundary conditions, the real part $\alpha$and imaginary part $\beta$ of the complex root of the characteristic equation, and constants $C_9$~$C_{12}$, can be solved, as expressed in Appendix 1 and 2, respectively.

The aforementioned derivations can also be applied to calculating the distributed uplift force of the simply supported SCCTB subjected to the other four loading types.

### *2.2.2 Two concentrated loads at the 1/3 beam span*

For the distributed uplift force of the simply supported SCCTB subjected to two concentrated loads at the 1/3 beam span $P_2$, the SCCTB can be divided into a pure bending segment, and two bending and shear segments.

For the bending and shear segment

$$r_1(x)=-\frac{na}{m+a^2}\left[C_{13}e^{\sqrt{a}x}+C_{14}e^{-\sqrt{a}x}\right] \tag{35}$$

$$r_2(x)=(C_{15}\cos\beta x+C_{16}\sin\beta x)e^{\alpha x}+(C_{17}\cos\beta x+C_{18}\sin\beta x)e^{-\alpha x} \tag{36}$$

where the expressions of the constants $C_{13}$ to $C_{18}$ are provided in Appendix 2.

For the pure bending segment

$$r_1(x)=-\frac{na}{m+a^2}\left[C_{19}e^{\sqrt{a}x}+C_{20}e^{-\sqrt{a}x}\right] \tag{37}$$

$$r_2(x)=(C_{21}\cos\beta x+C_{22}\sin\beta x)e^{\alpha x}+(C_{23}\cos\beta x+C_{24}\sin\beta x)e^{-\alpha x} \tag{38}$$

where the expressions of the constants $C_{19}$ to $C_{24}$ are provided in Appendix 2.

### *2.2.3 Uniformly distributed load*

For the distributed uplift force of the simply supported SCCTB subjected to the uniformly distributed load $q$

$$r_1(x)=-\frac{na}{m+a^2}\frac{gq}{a^2}\frac{e^{\sqrt{a}x}+e^{-\sqrt{a}x}}{e^{\sqrt{a}\frac{L}{2}}+e^{-\sqrt{a}\frac{L}{2}}}-\frac{q}{m}(l-\frac{ng}{a}) \tag{39}$$

$$r_2(x)=(C_{25}\cos\beta x+C_{26}\sin\beta x)e^{\alpha x}+(C_{27}\cos\beta x+C_{28}\sin\beta x)e^{-\alpha x} \tag{40}$$

where the expressions of $l$ and the constants$C_{25}$ to $C_{28}$ are provided in Appendix 1 and 2, respectively.

### *2.2.4 A concentrated load at the any position of the beam span*

For the distributed uplift force of the simply supported SCCTB subjected to a concentrated load at the any position of the beam span $P_3$

$$r_1(x)=\begin{cases}-\dfrac{na}{m+a^2}\left[C_{29}e^{\sqrt{a}x}+C_{30}e^{-\sqrt{a}x}\right],-L_1\le x\le 0\\ -\dfrac{na}{m+a^2}\left[C_{31}e^{\sqrt{a}x}+C_{32}e^{-\sqrt{a}x}\right],0\le x\le L_2\end{cases} \tag{41}$$

$$r_2(x)=(C_{33}\cos\beta x+C_{34}\sin\beta x)e^{\alpha x}+(C_{35}\cos\beta x+C_{36}\sin\beta x)e^{-\alpha x} \tag{42}$$

where the expressions of the constants $C_{29}$ to $C_{32}$ are provided in Appendix 2. However, the precise expressions of $C_{33}$ to $C_{36}$ in Eq. (42) are very complex; therefore, they are omitted in this paper.

### *2.2.5 Two concentrated loads at the symmetrical position of the beam span*

For the distributed uplift force of the simply supported SCCTB subjected to two concentrated loads at the symmetrical position of the beam span $P_4$, the SCCTB can be divided into a pure bending segment, and two bending and shear segments.

For the bending and shear segment

$$r_1(x)=-\frac{na}{m+a^2}\left[C_{37}e^{\sqrt{a}x}+C_{38}e^{-\sqrt{a}x}\right],\frac{L_1}{2}\le x\le\frac{L}{2} \tag{43}$$

$$r_2(x)=(C_{39}\cos\beta x+C_{40}\sin\beta x)e^{\alpha x}+(C_{41}\cos\beta x+C_{42}\sin\beta x)e^{-\alpha x} \tag{44}$$

where the expressions of the constants $C_{37}$ to $C_{42}$ are provided in Appendix 2.

For the pure bending segment

$$r_1(x)=-\frac{na}{m+a^2}\left[C_{43}e^{\sqrt{a}x}+C_{44}e^{-\sqrt{a}x}\right],0\le x\le\frac{L_1}{2} \tag{45}$$

$$r_2(x)=(C_{45}\cos\beta x+C_{46}\sin\beta x)e^{\alpha x}+(C_{47}\cos\beta x+C_{48}\sin\beta x)e^{-\alpha x} \tag{46}$$

where the expressions of the constants $C_{43}$ to $C_{48}$ are provided in Appendix 2.

## 3. Theoretical derivation of the deflection

Compared to the achievements of the traditional steel-concrete composite beam, the state of research in the SCCTB field currently remains under development. Moreover, theoretical studies on the SCCTB deflection are limited. In fact, the shear slip, uplift and shear effects may significantly affect the SCCTB deflection.

### 3.1 Basic assumptions

In order to derive the formulae for the SCCTB deflection, five basic assumptions are made, as follows.

(1) The formulae for calculating the SCCTB deflection are suitable for the steel truss and concrete slab in the elastic state, and the influence of concrete cracks is ignored.
(2) The influence of the geometrical nonlinearity of the steel truss on the SCCTB deflection is inconspicuous in its elastic state; hence, the geometrical nonlinearity of the steel truss is ignored.
(3) In the deflection calculation, the effective width of the concrete slab is considered.
(4) The shear resistance of the concrete slab and steel truss chords is omitted. The shear is only resisted by the steel truss braces; therefore, the shear effect plays an important role in the deflection calculation.
(5) The concrete is considered in compression only. Moreover, creep may significantly influence the mechanical behaviour of the concrete and is a long-term effect. In order to consider the creep effect, $I_c$ is redefined as the moment of inertia of the concrete slab cross-section with half of the effective width (GB 50017-2017).

In general, the deflection of the SCCTB, $y_d$, which considers the shear slip, uplift and shear effects, can be expressed by

$$y_d = y_{d1} + y_{d2} + y_{d3} + y_{d4} \tag{47}$$

where $y_{d1}$ is the deflection of the traditional steel-concrete composite beam with full shear interaction caused by the bending moment; $y_{d2}$ is the additional SCCTB deflection caused by the shear slip effect; $y_{d3}$ is the additional SCCTB deflection caused by the uplift effect; and $y_{d4}$ is the additional SCCTB deflection caused by the shear effect.

### 3.2 Determination of $y_{d1}$

The composite action of the traditional steel-concrete composite beam is realised by connecting two different material layers with shear connectors. Theoretically, if the shear connectors are rigid, full composite action can be achieved. In this case, the benefits of the composite action can be demonstrated in full when no slip deformation or deflection difference appears at the interface, which is referred to as full shear interaction. Meanwhile, the concrete is considered in compression only. For the creep effect, $I_c$ is redefined as the moment of inertia of the concrete slab cross-section with half of the effective width. Therefore, for the traditional steel-concrete composite beam with full shear interaction, the curvature $\varphi_F$ of the deformed steel truss is equal to that of the deformed concrete slab, as expressed in Eq. (48).

$$\varphi_F = \frac{M_c}{E_c I_c} = \frac{M_s}{E_s I_s} = \frac{M_c + M_s}{E_c I_c + E_s I_s} \tag{48}$$

The shear connectors exhibit infinite stiffness. Thus, $1/k_l = 0$ and $1/k_v = 0$, leading to $1/a = 0$ and $f/a = 0$. As a result, Eq. (21) can be simplified as

$$N = \frac{g}{a} M \tag{49}$$

By defining $EI = E_c I_c + E_s I_s$, and combining Eq. (48) with Eqs. (18) and (49), Eqs. (50) and (51) are obtained.

$$\varphi_F = \frac{M}{EID} \tag{50}$$

$$\frac{1}{D} = 1 - \frac{g}{a} H \tag{51}$$

For the simply supported SCCTB subjected to a concentrated load at the middle of the beam span $P_1$, the maximum deflection (Eq. (52))can be obtained based on the basic theory of structural mechanics and Eq. (50).

$$y_d = y_{d1} = \frac{P_1 L^3}{48DEI} \tag{52}$$

For the simply supported SCCTB subjected to two concentrated loads at the 1/3 beam span $P_2$, the maximum deflection (Eq. (53)) can be obtained based on the basic theory of structural mechanics and Eq. (50).

$$y_d = y_{d1} = \frac{23P_2 L^3}{648DEI} \tag{53}$$

For the simply supported SCCTB subjected to a uniformly distributed load $q$, the maximum deflection (Eq. (54)) can be obtained based on the basic theory of structural mechanics and Eq. (50).

$$y_d = y_{d1} = \frac{5qL^4}{384DEI} \tag{54}$$

For the simply supported SCCTB subjected to a concentrated load at any position of the beam span $P_3$, the maximum deflection (Eq. (55))can be obtained based on the basic theory of structural mechanics and Eq. (50).

$$y_d = y_{d1} = \frac{P_3 L_1^2 L_2^2}{3LDEI} \tag{55}$$

For the simply supported SCCTB subjected to two concentrated loads at a symmetrical position of the beam span $P_4$, the maximum deflection (Eq. (56)) can be obtained based on the basic theory of structural mechanics and Eq. (50).

$$y_d = y_{d1} = \frac{P_4}{EID}\left[\frac{L^3}{24} + \frac{L_1^3}{48} - \frac{PLL_1^2}{16}\right] \tag{56}$$

### *3.3 Determination of $y_{\mathrm{d}2}$*

As only the shear slip effect is considered, the axial stiffness of the shear connectors $k_v$ is infinite, while the shear stiffness of the shear connectors $k_l$ is finite. Therefore, $1/k_v = 0$, leading to $f = 0$ and $f/a = 0$. As a result, Eq. (21) can be simplified as

$$N = \frac{1}{a}\frac{d^2N}{dx^2} + \frac{g}{a}M \tag{57}$$

By combining Eq. (48) with Eqs. (18), (51) and (57), Eq. (58) is obtained

$$\frac{d^2y_d}{dx^2} = -\varphi_F = -\frac{M}{EID} + \frac{H}{aEI}\frac{d^2N}{dx^2} \tag{58}$$

In order to solve Eq. (58), the quadratic integral must be implemented. The solution to $y_d$ is illustrated in Eq. (59).

$$y_d = y_{d1} + y_{d2} = y_{d1} + \frac{H}{EIa}N(x) \tag{59}$$

For the simply supported SCCTB subjected to a concentrated load at the middle of the beam span $P_1$, according to the boundary conditions (Eqs. (60) and (61)) as well as Eqs. (26) and (30), the maximum deflection can be derived as expressed in Eq. (62).

$$y_d\big|_{x=L/2} = 0 \tag{60}$$

$$\left.\frac{dy_d}{dx}\right|_{x=0} = 0 \tag{61}$$

$$y_{d2} = \frac{H}{aEI}\left(\frac{P_1 g}{2a\sqrt{a}}\frac{1-e^{\sqrt{a}L}}{1+e^{\sqrt{a}L}} + \frac{gP_1L}{4a}\right) \tag{62}$$

Similar derivations can be applied to calculate the deflection of the simply supported SCCTB subjected to the other four loading types.

For the simply supported SCCTB subjected to two concentrated loads at the 1/3 beam span $P_2$, the maximum deflection is expressed as

$$y_{d2} = \frac{H}{aEI}\left(\frac{P_2 g}{a\sqrt{a}}\frac{e^{\frac{L\sqrt{a}}{6}} - e^{\frac{5L\sqrt{a}}{6}}}{1+e^{\sqrt{a}L}} + \frac{g}{a}\frac{P_2L}{3}\right) \tag{63}$$

For the simply supported SCCTB subjected to a uniformly distributed load $q$, the maximum deflection is expressed as

$$y_{d2} = \frac{H}{aEI}\left(\frac{gq}{a^2}\frac{2}{e^{\sqrt{a}\frac{L}{2}} + e^{-\sqrt{a}\frac{L}{2}}} + \frac{g}{a}\frac{qL^2}{8} - \frac{gq}{a^2}\right) \tag{64}$$

For the simply supported SCCTB subjected to a concentrated load at any position of the beam span $P_3$, the maximum deflection is expressed as

$$y_{d2} = \frac{H}{aEI}\left(\frac{P_3 g}{2a\sqrt{a}}\frac{e^{2\sqrt{a}L} + 1 - e^{2\sqrt{a}L_1} - e^{2\sqrt{a}L_2}}{1-e^{2\sqrt{a}L}} + \frac{gP_3L_1L_2}{aL}\right) \tag{65}$$

For the simply supported SCCTB subjected to two concentrated loads at a symmetrical position of the beam span $P_4$, the maximum deflection is expressed as

$$y_{d2} = \frac{H}{aEI}\left(\frac{P_4 g(e^{\frac{L_1}{2}\sqrt{a}} - e^{(L-\frac{L_1}{2})\sqrt{a}})}{2a\sqrt{a}(1+e^{L\sqrt{a}})} + \frac{gP_4L_2}{a}\right) \tag{66}$$

### *3.4 Determination of $y_{\mathrm{d}3}$*

When both the shear slip and uplift effects are considered, the differential equation for the deflection of the simply supported SCCTB is expressed as

$$\frac{d^2y_d}{dx^2} = -\frac{M_s}{E_sI_s} \tag{67}$$

By combining Eq. (67) with Eqs. (12), (20) and (21), Eq. (68) is obtained.

$$\frac{d^2y_d}{dx^2} = \frac{H}{EIa}\left(\frac{d^2N}{dx^2}\right) + \left(\frac{E_cI_cp}{EIk_v} + \frac{fH}{aEI}\right)\frac{d^2r}{dx^2} + \frac{M}{EI}\left(\frac{g}{a}H - 1\right) \tag{68}$$

According to the derivations in Sections 3.2 and 3.3, Eq. (68) can be changed as follows

$$y_d = y_{d1} + y_{d2} + \left(\frac{E_cI_cp}{EIk_v} + \frac{fH}{aEI}\right)r + Cx + D \tag{69}$$

Based on the boundary conditions (Eqs. (60) and (61)), the deflection of the simply supported SCCTB can be expressed as

$$\begin{aligned} y_d &= y_{d1} + y_{d2} + y_{d3} = y_{d1} + y_{d2} \\ &\quad + \left(\frac{E_cI_cp}{EIk_v} + \frac{fH}{aEI}\right)r(x) - \left(\frac{E_cI_cp}{EIk_v} + \frac{fH}{aEI}\right)r\left(\frac{L}{2}\right) \end{aligned} \tag{70}$$

For the simply supported SCCTB subjected to a concentrated load at the middle of the beam span $P_1$, the following is derived

$$y_{d3} = \left(\frac{E_cI_cp}{EIk_v} + \frac{fH}{aEI}\right)\left\{\frac{P_1\alpha\left[(e^{\alpha L} + e^{-\alpha L}) + 2\cos\beta L - 2\cos\beta\frac{L}{2}(e^{\alpha\frac{L}{2}} + e^{-\alpha\frac{L}{2}})\right]}{(e^{\alpha L} - e^{-\alpha L}) + \sin\alpha L}\right\} \tag{71}$$

F For the simply supported SCCTB subjected to two concentrated loads at the 1/3 beam span $P_2$, the following is derived

$$y_{d3}=(\frac{E_cI_cp}{EIk_v}+\frac{fH}{aEI})\left[\frac{2P_2\alpha(e^{\alpha L}+e^{-\alpha L})+4P_2\alpha\cos\beta L}{\Delta_1}-2C_{15}\right] \quad (72)$$

For the simply supported SCCTB subjected to a uniformly distributed load $q$, the following is derived

$$y_{d3}=(\frac{E_cI_cp}{EIk_v}+\frac{fH}{aEI})\left[\frac{qL\alpha\left[(e^{\alpha L}+e^{-\alpha L})+2\cos\beta L-2\cos\beta\frac{L}{2}(e^{\alpha\frac{L}{2}}+e^{-\alpha\frac{L}{2}})\right]}{(e^{\alpha L}-e^{-\alpha L})+\sin\alpha L}\right] \quad (73)$$

For the simply supported SCCTB subjected to a concentrated load at any position of the beam span $P_3$, the following is derived

$$y_{d3}=(\frac{E_cI_cp}{EIk_v}+\frac{fH}{aEI})\left[2P_3\alpha\frac{L_1^2+L_2^2}{L^2}\right] \quad (74)$$

For the simply supported SCCTB subjected to two concentrated loads at a symmetrical position of the beam span $P_4$, the following is derived

$$y_{d3}=(\frac{E_cI_cp}{EIk_v}+\frac{fH}{aEI})\left[\frac{2P_4\alpha(e^{\alpha L}+e^{-\alpha L})+4P_4\alpha\cos\beta L}{\Delta_3}-2C_{45}\right] \quad (75)$$

### 3.5 Determination of $y_{d4}$

The shear is only resisted by the steel truss braces. Therefore, in the derivation of $y_{d4}$, the contributions of the steel truss chords and concrete slab are ignored. Moreover, the deformation of the braces may add to the SCCTB deflection and the shear effect can also not be ignored. According to the basic theory of structural mechanics (Long *et al*. 2012), the additional SCCTB deflection caused by the shear effect can be calculated, as expressed in Eq. (76).

$$y_{d4}=\sum_{i=1}^{n}\frac{F_iF_{1i}l_i}{E_sA_i} \quad (76)$$

where $F_i$ is the axial force of the $i^{th}$ brace under the external load; $F_{1i}$ is the axial force of the $i^{th}$ brace under the unit load applied to the position with maximum deflection; $l_i$ is the length of the $i^{th}$ brace; and $A_i$ is the area of the $i^{th}$ brace.

### 3.6 Practical design method

It can be observed that the formulae for calculating $y_{d2}$ and $y_{d3}$ are complex. As $e^{-\sqrt{a}L}\approx 0$ and $e^{-aL}\approx 0$, the corresponding formulae can be simplified. The formulae for calculating the SCCTB deflection are listed in Table 1.

The formulae listed in Table 1 are mainly derived based on the differential, equilibrium and deformation compatibility equations. However, the solutions to these equations differ owing to the varying loading types. Therefore, a practical design method (Eqs. (76) to (79)) is proposed to provide an effective and convenient tool for designers to estimate the SCCTB deflection.

For the deflection $y_{d1}$, the formulae for the SCCTB under five different loading types can be simplified as

$$y_{d1}=\frac{\delta M_dL^2}{EID} \quad (77)$$

where $\delta$ is a constant related to the loading types and can be determined by the basic theory of structural mechanics; and $M_d$ is the bending moment at the position corresponding to the maximum deflection.

For the deflection $y_{d2}$, the formulae for the SCCTB under five different loading types can be simplified as

$$y_{d2}=\frac{gH}{a^2EI}(-\frac{\sum_{i=1}^{n}P_ie^{-\sqrt{a}L_i}}{2\sqrt{a}}+M_d) \quad (78)$$

where $i$ is the amount of concentrated loads; and $L_i$ is the distance between the loading position of $P_i$ and the position corresponding to the maximum deflection.

For the deflection $y_{d3}$, the formulae for the SCCTB under five different loading types can be simplified as

$$y_{d3}=2\alpha(\frac{E_cI_cp}{EIk_v}+\frac{fH}{aEI})(\frac{L_BV_A+L_AV_B}{L}) \quad (79)$$

Table 1 Formulae for calculating the deflection of the SCCTB

| Loading types | $y_{d1}$ | $y_{d2}$ | $y_{d3}$ | $y_{d4}$ |
|---|---|---|---|---|
| $P_1$ | $\frac{P_1L^3}{48DEI}$ | $\frac{H}{aEI}(-\frac{P_1g}{2a\sqrt{a}}+\frac{gP_1L}{4a})$ | $(\frac{E_cI_cp}{EIk_v}+\frac{fH}{aEI})P_1\alpha$ | $\sum_{i=1}^{n}\frac{F_iF_{1i}l_i}{E_sA_i}$ |
| $P_2$ | $\frac{23P_2L^3}{648DEI}$ | $\frac{H}{aEI}(-\frac{P_2g}{a\sqrt{a}}e^{-\frac{\sqrt{a}L}{6}}+\frac{gP_2L}{3a})$ | $(\frac{E_cI_cp}{EIk_v}+\frac{fH}{aEI})2P_2\alpha$ | $\sum_{i=1}^{n}\frac{F_iF_{1i}l_i}{E_sA_i}$ |
| $q$ | $\frac{5qL^4}{384DEI}$ | $\frac{H}{aEI}(-\frac{qg}{a^2}+\frac{gqL^2}{8a})$ | $(\frac{E_cI_cp}{EIk_v}+\frac{fH}{aEI})qL\alpha$ | $\sum_{i=1}^{n}\frac{F_iF_{1i}l_i}{E_sA_i}$ |
| $P_3$ | $\frac{P_3L_1^2L_2^2}{3LDEI}$ | $\frac{H}{aEI}(-\frac{P_3g}{2a\sqrt{a}}+\frac{gP_3L_1L_2}{aL})$ | $(\frac{E_cI_cp}{EIk_v}+\frac{fH}{aEI})\left[2P_3\alpha\frac{L_1^2+L_2^2}{L^2}\right]$ | $\sum_{i=1}^{n}\frac{F_iF_{1i}l_i}{E_sA_i}$ |
| $P_4$ | $\frac{P_4}{EID}\left[\frac{L^3}{24}+\frac{L_1^3}{48}-\frac{PLL_1^2}{16}\right]$ | $\frac{H}{aEI}(-\frac{P_4g}{a\sqrt{a}}e^{-\frac{\sqrt{a}L_1}{2}}+\frac{gP_4L_2}{a})$ | $(\frac{E_cI_cp}{EIk_v}+\frac{fH}{aEI})2P_4\alpha$ | $\sum_{i=1}^{n}\frac{F_iF_{1i}l_i}{E_sA_i}$ |

where $L_A$ and $L_B$ are the distances between the supports and position corresponding to the maximum deflection; and $V_A$ and $V_B$ are the vertical reaction forces of the supports.

For the deflection $y_{d4}$, this additional SCCTB deflection under five different loading types is calculated using the same formula as Eq. (76).

## 4. Experimental results and validation

In order to validate the reliability of the proposed formulae, an experimental program was carried out on the flexural response of three SCCTB specimens with different stud connector distributions. In the following section, the test specimen dimensions and parameters, material properties, measured points, test setup and instrumentation, test procedure and phenomena, and a comparison of the theoretical and experimental results are described in details.

### *4.1 Specimens*

The degree of shear connection was the main factor in the experimental program; therefore, three SCCTB specimens were designed for the flexural tests. The dimensions of the SCCTB specimens are plotted in Fig. 3.

The square pyramid structure was selected for the steel truss in order to obtain sufficient lateral stiffness. The steel truss height and span were 500 and 4000 mm, respectively. A circular tube was selected for the steel member to obtain improved stability performance. The upper chord, bottom chord and brace dimensions were $\phi42\times3$, $\phi70\times5$ and $\phi32\times4$ mm$^2$, respectively. These members were connected by means of a fillet weld. The concrete slab thickness and width were 80 and 1500 mm, respectively. Two pieces of reinforcement grid were placed at the top and bottom of the concrete slab. A longitudinal reinforcement with a 6 mm nominal diameter and 100 mm spacing, and transverse reinforcement with a 6 mm nominal diameter and 150 mm spacing were adopted for the reinforcement grid. Stud connectors with a diameter of 13 mm and design strength of 215 MPa were used to connect the steel truss and concrete slab. Three stud connector distributions were designed, as listed in Table 2, where $k$ is the shear interaction factor and equal to the ratio of $n_s$ to $n_r$; $n_r$ is the critical amount of stub connectors between the full and partial shear interaction; and $n_s$ is the actual amount of stub connectors. The critical amount of stub connectors between the full and partial shear interaction was 34. The SCCTB specimens are illustrated in Fig. 4.

### *4.2 Materials*

The steel members were manufactured from Q345B steel (the nominal yield strength of which is 345 MPa). Three tensile coupons were directly and randomly cut from the bottom chords. Moreover, three reinforcement coupons with a 60 mm length and 6 mm nominal diameter were designed. Tensile coupon tests were conducted to determine the mechanical properties of the steel members and

Table 2 Three distributions of the stud connectors

| No. | Span / mm | $k$ | $n_s$ | $p$ |
|---|---|---|---|---|
| SCCTB1 | 4000 | 0.88 | 30 | 300 |
| SCCTB2 | 4000 | 1.0 | 34 | 250 |
| SCCTB3 | 4000 | 1.24 | 42 | 200 |

Fig. 4 SCCTB specimens

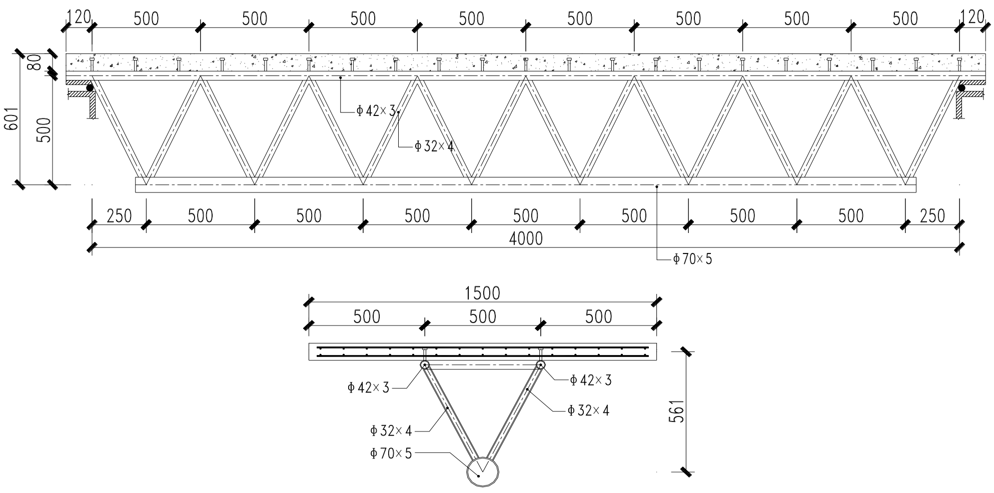


Fig. 3 Dimensions of the SCCTB specimens

Table 3 Material properties of the steel members and reinforcement bars

| Material | Tensile coupon | $f_y$ / MPa | $f_u$ / MPa | Elongation |
|---|---|---|---|---|
| Steel members | Coupon 1 | 432.4 | 535.7 | 0.292 |
| | Coupon 2 | 438.3 | 537.6 | 0.287 |
| | Coupon 3 | 440.4 | 542.4 | 0.283 |
| | Mean | 437.0 | 538.6 | 0.287 |
| Reinforcement bar | Coupon 1 | 414.0 | 559.1 | 0.322 |
| | Coupon 2 | 406.9 | 548.5 | 0.318 |
| | Coupon 3 | 396.3 | 544.9 | 0.315 |
| | Mean | 405.7 | 550.8 | 0.318 |

Table 4 Material properties of the concrete

| Concrete cube | $f_{cu,0}$ / MPa | $f_c$ / MPa | $E_c$ / MPa |
|---|---|---|---|
| Cube 1 | 34.9 | 23.3 | 31306 |
| Cube 2 | 35.2 | 23.5 | 31389 |
| Cube 3 | 34.8 | 23.3 | 31278 |
| Mean | 35.0 | 23.4 | 31324 |

reinforcement bars. The measured yield strength $f_y$, ultimate strength $f_u$ and elongation of the steel members and reinforcement bars are listed in Table 3.

Ordinary concrete of C30 strength grade was selected as the concrete slab material. The mix proportion of the concrete was cement to sand to coarse aggregate to water = 1:1.6:3:0.5. In order to obtain the concrete mechanical properties, three concrete cubes with dimensions of 150 × 150 × 150 mm were designed and compressive concrete cube tests were conducted. The measured properties of these concrete cubes are displayed in Table 4.

### *4.3 Measured points*

The linear variable differential transducers (LVDTs) used are illustrated in Fig. 5. Vertical LVDTs were located at the 1/8, 1/4, 3/8, 1/2, 5/8, 3/4 and 7/8 positions along the SCCTB specimen length to measure the deflection. Vertical LVDTs were placed on the concrete slab bottom surface and steel truss upper chord of the steel truss. Moreover, two vertical LVDTs were placed on the SCCTB specimen supports to obtain their displacement. A total of 16 vertical LVDTs were required for each flexural test.

### *4.4 Test setup and instrumentation*

A self-balancing reaction frame was designed for the experimental studies on the SCCTB flexural response. All of the SCCTB specimens were installed in the same test setup, as illustrated in Fig. 6. A concentrated load was applied in the middle of the concrete slab by means of a 1000 kN hydraulic jack. Two rods were placed at the two ends of the SCCTB specimens to simulate the hinged supports.

Fig. 5 LVDTs

(a) Hinged support

(b) A self-balancing reaction frame

Fig. 6 Test setup of the SCCTB specimens

### *4.5 Test procedure and deformation phenomena*

Following installation of each SCCTB specimen and the measuring equipment, the test equipment was checked by means of trial loading. A preload, which was 10 to 20% of the ultimate load, was applied to ensure that these SCCTB specimens and the test equipment were operating correctly. The ultimate load was initially estimated according to the finite element results. Once everything had been examined, the tests were started. The load increment was 20 kN/min when the SCCTB specimens were in the elastic phase. For each loading level, the load was required to be sustained for 3 min to record stable data. The test was conducted under force control at the beginning of the loading process. When the deformation of the SCCTB specimens increased rapidly, the behaviour of the SCCTB specimens entered the nonlinear region. At this time, the force control was changed to displacement control, until failure of the SCCTB specimens occurred. The displacement increment was 5 mm.

The deformation phenomena of the SCCTB specimens roughly progressed through three phases, as follows. (1) At the beginning of the loading process, the deformation of the SCCTB specimens was inconspicuous, signifying the elastic phase. (2) As the load increased, the behaviour of the SCCTB specimens entered the nonlinear region, leading to rapid development in their deformation. (3) When the load increased to approximately 85% of the ultimate load, cracks appeared on the bottom surface of the concrete slab. The cracks initially appeared in the middle area of the concrete slab corresponding to the truss joint. Subsequently, cracks also appeared in the connection area of the stub connectors. The amount of cracks increased with the increase in the load. Finally, the cracks expanded and ran through the concrete slab, as illustrated in Figs. 7 and 8. The final flexural deformation of the SCCTB specimens is illustrated in Fig. 9.

Fig. 7 Cracks at the bottom of the concrete slab

Fig. 8 Cracks at the edge of the concrete slab

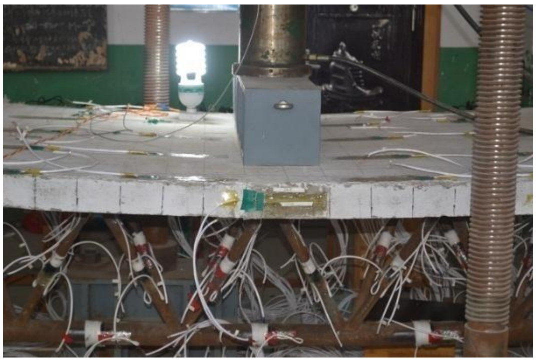

Fig. 9 Final deformation of the SCCTB specimens

### *4.6 Load-deflection curves*

The load-deflection curves of the SCCTB specimens are plotted in Fig. 10. When the load was smaller than 200 kN, the load-deflection curves of the specimens exhibited a linear response and were very close, indicating that the SCCTB specimens remained in the elastic phase. As the load increased, the load-deflection curves separated. It can be observed that the stiffness of specimen SCCTG1 decreased most rapidly with the lowest ultimate load of 385.6 kN, while specimen SCCTG3 exhibited the largest ultimate load of 408.7 kN. Therefore, the distribution of the stud connectors had an effect on the SCCTB mechanical behaviour. The stiffness and ultimate load of the SCCTB increased with an increase in the shear interaction factor *k*.

### *4.7 Comparison of theoretical and experimental results*

The deflection of the SCCTB specimens obtained from the proposed formulae was validated by means of the experimental results, as presented in Table 5. The load corresponding to the deflection listed in Table 5 is 120 kN. It can be observed that: (1) the deflection obtained from both the proposed formulae and experimental results exhibited an obvious decrease with an increase of the shear interaction factor *k*; (2) the average deviation of the deflection between the theoretical and experimental results was 3.6%; and (3) the experimental deflection was smaller than the theoretical deflection. Consequently, strong

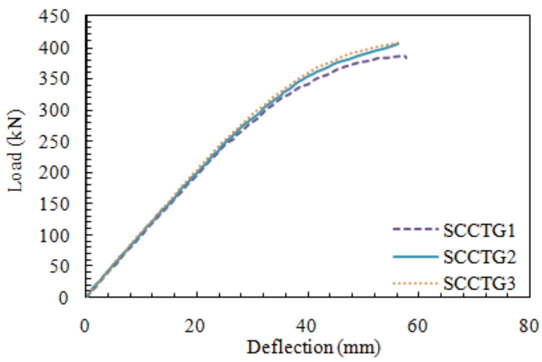


Fig. 10 Load-deflection curves

Table 5 Deflection of the SCCTB specimens

| No. | Test (mm) | Formulae (mm) | | | | | Deviation |
|---|---|---|---|---|---|---|---|
| | | $y_{d1}$ | $y_{d2}$ | $y_{d3}$ | $y_{d4}$ | $y_d$ | |
| SCCTB 1 | 11.92 | 4.73 | 1.16 | 0.86 | 5.62 | 12.37 | 3.6% |
| SCCTB 2 | 11.65 | 4.73 | 1.05 | 0.63 | 5.62 | 12.03 | 3.2% |
| SCCTB 3 | 11.43 | 4.73 | 0.98 | 0.56 | 5.62 | 11.89 | 3.9% |
| Mean | | | | | | | 3.6% |

agreement was demonstrated in the validation of the proposed formulae against the representative experimental results. Therefore, the formulae proposed in this paper can be used to predict the SCCTB deflection with confidence and safety.

## 5. Conclusions

The uplift force of the stud connectors was derived based on the differential and equilibrium equations. Subsequently, considering the shear slip, uplift and shear effects, a practical design method was developed for calculating the deflection in the serviceability limit state of the SCCTB under five different loading types. In order to validate the practical design method, flexural tests were carried out on three SCCTBs. It is found that the distribution of the stud connectors could affect the mechanical behaviour of the SCCTB. The stiffness and ultimate load of the SCCTB increased with an increase in the shear interaction factor. The proposed formulae were calibrated by means of the experimental results, and provide an effective, acceptable and convenient method for designers to calculate the maximum deflection of a simply supported SCCTB.

## Acknowledgments

The authors gratefully acknowledge the financial support provided by the National Science Foundation of Hainan Province of China (Project No. 518QN213), the National Natural Science Foundation of China (Project No. 51478437) and the Major Science and Technology Special Foundation of Zhengzhou (Project No. 152PZDZX033).

## References

Amadio, C., Fragiacomo, M. and Macorini, L. (2012), "Evaluation of the deflection of steel-concrete composite beams at serviceability limit state", *J. Constr. Steel Res.*, **7**3, 95-104.

Ding, F.X., Liu, J., Liu, X.M., Yu, Z.W. and Li, Y.S. (2018), "Experimental investigation on hysteretic behavior of simply supported steel-concrete composite beam", *J. Constr. Steel Res.*, **144**, 153-165.

Elmatzoglou, M. and Avdelas, A. (2017), "Numerical Modelling of Double-Steel Plate Composite Shear Walls", *Computation*, **5**(1), 12.

El-Zohairy, A., Salim, H., Shaaban, H., Mustafa, S. and El-Shihy, A. (2017), "Experimental and FE parametric study on continuous steel-concrete composite beams strengthened with CFRP laminates", *Constr. Build. Mater.*, **157**, 885-898.

GB 50017-2017 (2017), Standard for design of steel structures; Ministry of housing and urban-rural development of the people's republic of China, General administration of quality supervision, inspection and quarantine of the People's Republic of China.

Goncalves, R. (2018), "An improved geometrically exact planar beam finite element for curved steel and steel-concrete composite beams", *Thin-Wall. Struct.*, **123**, 492-500.

Henderson, I.E.J., Zhu, X.Q., Uy, B. and Mirza, O. (2015), "Dynamic behaviour of steel-concrete composite beams with different types of shear connectors. Part I: Experimental study", *Eng. Struct.*, **103**, 298-307.

Huang, Y.J., Xiao, J.Z. and Shen, L. (2016), "Damage assessment for seismic response of recycled concrete filled steel tube columns", *Earthq. Eng. Eng. Vib.*, **15**(3), 607-616.

Jiang, S., Guo, X., Xiong, Z., Cai, Y. and Zhu, S. (2017), "Experimental studies on behaviour of tubular T-joints reinforced with grouted sleeve", *Steel Compos. Struct., Int. J.*, **23**(5), 585-596.

Jiang, L.Z., Feng, Y.L. and Zhou, W.B. (2018), "Analysis on natural vibration characteristics of steel-concrete composite truss beam", *Steel Compos. Struct., Int. J.*, **26**(1), 79-87.

Karam, E.C., Hawileh, R.A., El Maaddawy, T. and Abdalla, J.A. (2017), "Experimental investigations of repair of pre-damaged steel-concrete composite beams using CFRP laminates and mechanical anchors", *Thin-Wall. Struct.*, **112**, 107-117.

Katwal, U., Tao, Z. and Hassan, M.K. (2018), "Finite element modelling of steel-concrete composite beams with profiled steel sheeting", *J. Constr. Steel Res.*, **146**, 1-15.

Lai, Z., Jiang, L., Zhou, W. and Chai, X. (2017), "Improved finite beam element method to analyze the natural vibration of steel-concrete composite truss beam", *Shock Vib.*, 5323246.

Liu, X., Bradford, M.A., Chen, Q.J. and Ban, H. (2016), "Finite element modelling of steel-concrete composite beams with high-strength friction-grip bolt shear connectors", *Finite Elem. Anal. Des.*, **108**, 54-65.

Liu, X.P., Bradford, M.A. and Ataei, A. (2017), "Flexural performance of innovative sustainable composite steel-concrete beams", *Eng. Struct.*, **130**, 282-296.

Long, Y.Q., Bao, S.H., Kuang, W.Q. and Yuan, S. (2012), *Structural Mechanics I-Basic Tutorials*, Higher Education Press, Beijing, China.

Lou, T.J., Lopes, S.M.R. and Lopes, A.V. (2016), "Numerical modeling of externally prestressed steel-concrete composite beams", *J. Struct. Eng.*, **121**, 229-236.

Luo, Y., Guo, X., Li, J., Xiong, Z., Meng, L., Dong, N. and Zhang, J. (2015), "Experimental research on seismic behaviour of the concrete-filled double-steel-plate composite wall", *Adv. Struct. Eng.*, **18**(11), 1845-1858.

Machacek, J. and Cudejko, M. (2013), "Design of shear connection between steel truss and concrete slab", *Procedia Eng.*, **57**, 722-729.

Machacek, J. and Charvat, M. (2017), "Study on shear connection of bridge steel truss and concrete slab deck", *J. Civil Eng. Manag.*, **23**(1), 105-112.

Pathirana, S.W., Uy, B., Mirza, O. and Zhu, X. (2016), "Flexural behaviour of composite steel-concrete beams utilising blind bolt shear connectors", *Eng. Struct.*, **114**, 181-194.

Song, A., Wan, S., Jiang, Z. and Xu, J. (2018), "Residual deflection analysis in negative moment regions of steel-concrete composite beams under fatigue loading", *Constr. Build. Mater.*, **158**, 50-60.

Subhani, M., Al-Ameri, R. and Kabir, M.I. (2018), "Hybrid strengthening of steel-concrete composite beam, part 1: Experimental investigation", *J. Constr. Steel Res.*, **141**, 23-25.

Uddin, M.A., Sheikh, A.H., Brown, D., Bennett, T. and Uy, B. (2018), "Geometrically nonlinear inelastic analysis of steel-concrete composite beams with partial interaction using a higher-order beam theory", *Int. J. Non-Linear Mech.*, **100**, 34-47.

Wen, J., Sheikh, A.H., Uddin, M.A. and Uy, B. (2018), "Analytical model for flexural response of two-layered composite beams with interfacial shear slip using a higher order beam theory", *Compos. Struct.*, **184**, 789-799.

Xian, Q., Tong, L., Zhou, L. and Chen, Y. (2017), "Experimental investigation on fatigue strength of joints between SRC beams and concrete-filled RHS columns", *KSCE J. Civil Eng.*, **21**(5),

1802-1811.
Yin, G.A., Ding, F.X., Wang, H.B., Bai, Y. and Liu, X.M. (2017), "Connection performance in steel–concrete composite truss bridge structures", *J. Bridge Eng.*, **22**(3), 04016126.
Xiong, M.X. and Liew, J.Y.R. (2016), "Mechanical bahviour of ultra-high strength concrete at elevated temperatures and fire resistance of ultra-high strength concrete filled steel tubes", *Mater. Des.*, **104**, 414-427.
Xiong, Z., Guo, X., Luo, Y. and Zhu, S. (2017), "Elasto-plastic stability of single-layer reticulated shells with aluminium alloy gusset joints", *Thin-wall. Struct.*, **115**, 163-175.
Zhang, F., Lu, Y., Li, S. and Zhang, W. (2018), "Eccentrically compressive behaviour of RC square short columns reinforced with a new composite mehtod", *Steel Compos. Struct., Int. J.*, **27**(1), 95-108.
Zhu, L., Nie, J.G., Li, F.X. and Ji, W.Y. (2015), "Simplified analysis method accounting for shear-lag effect of steel-concrete composite decks", *J. Struct. Eng.*, **115**, 62-80.

*CC*

## Notation

| | Explanation |
|---|---|
| $P_1$ | A concentrated load at the middle of the beam span |
| $P_2$ | Two concentrated loads at the 1/3 beam span |
| $P_3$ | A concentrated load at any position of the beam span |
| $P_4$ | Two concentrated loads at a symmetrical position of the beam span |
| $q$ | A uniformly distributed load |
| $b_1$ | The distance from the centroidal axis to the concrete slab bottom |
| $b_2$ | The distance from the centroidal axis to the concrete slab top |
| $h_1$ | The distance from the centroidal axis to the steel truss top |
| $h_2$ | The distance from the centroidal axis to the steel truss bottom |
| $N_c$ | The axial force applied to the concrete slab |
| $N_s$ | The axial force applied to the steel truss |
| $M_c$ | The bending moment acting on the concrete slab |
| $M_s$ | The bending moment acted on the steel truss |
| $V_c$ | The shear force applied to the concrete slab |
| $V_s$ | The shear force applied to the steel truss |
| $r$ | The distributed uplift force applied to the continuous elastic material used to replace the stud connectors |
| $r_1(x)$ | The particular solution of $r$ |
| $r_2(x)$ | The general solution of $r$ |
| $u$ | The distributed shear force applied to the continuous elastic material used to replace the stud connectors |
| $S$ | The slip deformation between the steel truss and concrete slab |
| $w$ | The deflection difference between the steel truss and concrete slab |
| $R$ | The uplift force applied to a single stud connector |
| $p$ | The longitudinal spacing of the stud connectors |
| $k_v$ | The axial stiffness of the stub connectors |
| $y_s$ | The deflection of the steel truss |
| $y_c$ | The deflection of the concrete slab |
| $E_c$ | The elastic modulus of concrete |
| $E_s$ | The elastic modulus of steel |
| $I_c$ | The moment of inertia of the concrete slab cross-section with an effective width |
| $I_s$ | The moment of inertia of the steel truss cross-section |
| $N$ | $N = N_s = N_c$ |
| $Q$ | The shear force applied to a single stud connector |
| $k_l$ | The shear stiffness of the stub connectors |
| $M$ | The external bending moment applied to the SCCTB |
| $H$ | The distance from the centroid of the steel truss cross-section to the centroid of the concrete slab cross-section |
| $C_i$ | The constants that can be determined by the boundary conditions |
| $\lambda_1$ | The real root of the characteristic equation |
| $\alpha$ | The real part of the complex root of the characteristic equation |
| $\beta$ | The imaginary part of the complex root of the characteristic equation |
| $y_d$ | The deflection of the SCCTB, which considers the shear slip, uplift and shear effects |
| $y_{d1}$ | The deflection of the traditional steel-concrete composite beam with full shear interaction caused by the bending moment |
| $y_{d2}$ | The additional SCCTB deflection caused by the shear slip effect |
| $y_{d3}$ | The additional SCCTB deflection caused by the uplift effect |
| $y_{d4}$ | The additional SCCTB deflection caused by the shear effect |
| $\varphi_F$ | The curvature of the deformed steel truss and deformed concrete slab |
| $F_i$ | The axial force of the $i^{th}$ brace under the external load |
| $F_{1i}$ | The axial force of the $i^{th}$ brace under the unit load applied to the position with maximum deflection |
| $l_i$ | The length of the $i^{th}$ brace |
| $A_i$ | The area of the $i^{th}$ brace |
| $\delta$ | A constant related to the loading types |
| $M_d$ | The bending moment at the position corresponding to the maximum deflection |
| $L_i$ | The distance between the loading position of $P_i$ and the position corresponding to the maximum deflection |
| $L_A$ | The distance between the support A and the position corresponding to the maximum deflection. |
| $L_B$ | The distance between the support B and the position corresponding to the maximum deflection. |
| $V_A$ | The vertical reaction force of the support A |
| $V_B$ | The vertical reaction force of the support B |

## Appendix A

$$m=\frac{k_v}{p}\left(\frac{1}{E_cI_c}+\frac{1}{E_sI_s}\right) \tag{80}$$

$$n=\frac{k_v}{p}\left(\frac{b_1}{E_cI_c}-\frac{h_1}{E_sI_s}\right) \tag{81}$$

$$a=\frac{k_l}{p}\left(\frac{1}{E_cA_c}+\frac{1}{E_sA_s}+\frac{H^2}{E_cI_c+E_sI_s}\right) \tag{82}$$

$$f=\frac{k_l}{k_v}\frac{-E_cI_ch_1+E_sI_sb_1}{E_cI_c+E_sI_s} \tag{83}$$

$$g=\frac{k_l}{p}\frac{H}{E_cI_c+E_sI_s} \tag{84}$$

$$A=\frac{k_l}{p}\frac{(E_sI_sb_1-E_cI_ch_1)^2}{(E_sI_s+E_cI_c)E_sI_sE_cI_c}+\frac{k_l}{p}\left(\frac{1}{E_cA_c}+\frac{1}{E_sA_s}+\frac{H^2}{E_cI_c+E_sI_s}\right) \tag{85}$$

$$B=\frac{k_v}{p}\left(\frac{1}{E_cI_c}+\frac{1}{E_sI_s}\right) \tag{86}$$

$$C=\frac{k_vk_l}{p^2}\left(\frac{1}{E_cI_c}+\frac{1}{E_sI_s}\right)\left(\frac{1}{E_cA_c}+\frac{1}{E_sA_s}+\frac{H^2}{E_cI_c+E_sI_s}\right) \tag{87}$$

$$\alpha=\beta=\frac{\sqrt[4]{m}}{\sqrt{2}} \tag{88}$$

$$l=\frac{k_v}{pE_cI_c} \tag{89}$$

## Appendix B

$$\begin{cases} C_7=\dfrac{P_1g}{2a\sqrt{a}(1+e^{\sqrt{a}L})} \\ C_8=-\dfrac{P_1g}{2a\sqrt{a}(1+e^{-\sqrt{a}L})} \end{cases} \tag{90}$$

$$\begin{cases} C_9=C_{10}=-\dfrac{P_1\alpha\cos\beta\frac{L}{2}(e^{\alpha\frac{L}{2}}+e^{-\alpha\frac{L}{2}})}{(e^{\alpha L}-e^{-\alpha L})+\sin\alpha L} \\ C_{11}=-C_{12}=-\dfrac{P_1\alpha\sin\beta\frac{L}{2}(e^{\alpha\frac{L}{2}}-e^{-\alpha\frac{L}{2}})}{(e^{\alpha L}-e^{-\alpha L})+\sin\alpha L} \end{cases} \tag{91}$$

$$\begin{cases} C_{13}=-\dfrac{P_2g}{2a\sqrt{a}}\dfrac{e^{\frac{L\sqrt{a}}{6}}+e^{-\frac{L\sqrt{a}}{6}}}{1+e^{\sqrt{a}L}} \\ C_{14}=\dfrac{P_2g}{2a\sqrt{a}}\dfrac{e^{\frac{L\sqrt{a}}{6}}+e^{-\frac{L\sqrt{a}}{6}}}{1+e^{-\sqrt{a}L}} \end{cases} \tag{92}$$

$$\begin{cases} C_{15}=C_{17}=-\dfrac{2P_2\alpha\cos\beta\frac{L}{2}(e^{\alpha\frac{L}{2}}+e^{\alpha\frac{L}{2}})}{\Delta_1} \\ C_{16}=-C_{18}=-\dfrac{2P_2\alpha\sin\beta\frac{L}{2}(e^{\alpha\frac{L}{2}}-e^{\alpha\frac{L}{2}})}{\Delta_1} \end{cases} \tag{93}$$

$$C_{19}=C_{20}=\frac{P_2g}{2a\sqrt{a}}\frac{e^{\frac{L\sqrt{a}}{6}}-e^{\frac{5L\sqrt{a}}{6}}}{1+e^{\sqrt{a}L}} \tag{94}$$

$$\begin{cases} C_{21}=C_{23}=C_{15}\Delta_2\left[\cos\beta\frac{L}{6}(e^{\frac{\alpha L}{6}}-e^{-\frac{\alpha L}{6}})-\sin\beta\frac{L}{6}(e^{\frac{\alpha L}{6}}+e^{-\frac{\alpha L}{6}})\right] \\ C_{22}=-C_{24}=C_{15}\Delta_2\left[\cos\beta\frac{L}{6}(e^{\frac{\alpha L}{6}}-e^{-\frac{\alpha L}{6}})+\sin\beta\frac{L}{6}(e^{\frac{\alpha L}{6}}+e^{-\frac{\alpha L}{6}})\right] \end{cases} \tag{95}$$

$$\begin{cases} C_{25}=C_{27}=-\dfrac{\alpha\cos\beta\frac{L}{2}(e^{\alpha\frac{L}{2}}+e^{\alpha\frac{L}{2}})}{(e^{\alpha L}-e^{-\alpha L})+\sin\alpha L}\dfrac{qL}{2} \\ C_{26}=-C_{28}=-\dfrac{\alpha\sin\beta\frac{L}{2}(e^{\alpha\frac{L}{2}}-e^{\alpha\frac{L}{2}})}{(e^{\alpha L}-e^{-\alpha L})+\sin\alpha L}\dfrac{qL}{2} \end{cases} \tag{96}$$

$$\begin{cases} C_{29}=\dfrac{P_3g(e^{2L\sqrt{a}}-e^{2L_1\sqrt{a}})}{2a\sqrt{a}(1-e^{2L\sqrt{a}})} \\ C_{30}=\dfrac{P_3g(1-e^{2L_2\sqrt{a}})}{2a\sqrt{a}(1-e^{2L\sqrt{a}})} \\ C_{31}=\dfrac{P_3g(1-e^{2L_1\sqrt{a}})}{2a\sqrt{a}(1-e^{2L\sqrt{a}})} \\ C_{32}=\dfrac{P_3g(e^{2L\sqrt{a}}-e^{2L_2\sqrt{a}})}{2a\sqrt{a}(1-e^{2L\sqrt{a}})} \end{cases} \tag{97}$$

$$\begin{cases} C_{37} = \dfrac{P_4 g(e^{\frac{L_1}{2}\sqrt{a}} + e^{-\frac{L_1}{2}\sqrt{a}})}{2a\sqrt{a}(1+e^{L\sqrt{a}})} \\ C_{38} = -\dfrac{P_4 g(e^{\frac{L_1}{2}\sqrt{a}} + e^{-\frac{L_1}{2}\sqrt{a}})}{2a\sqrt{a}(1+e^{-L\sqrt{a}})} \end{cases} \tag{98}$$

$$\begin{cases} C_{39} = C_{41} = -\dfrac{2P_4\alpha\cos\beta\dfrac{L}{2}(e^{\alpha\frac{L}{2}} + e^{\alpha\frac{L}{2}})}{\Delta_3} \\ C_{40} = -C_{42} = -\dfrac{2P_4\alpha\sin\beta\dfrac{L}{2}(e^{\alpha\frac{L}{2}} - e^{\alpha\frac{L}{2}})}{\Delta_3} \end{cases} \tag{99}$$

$$C_{43} = C_{44} = \frac{Pg(e^{\frac{L_1}{2}\sqrt{a}} - e^{(L-\frac{L_1}{2})\sqrt{a}})}{2a\sqrt{a}(1+e^{L\sqrt{a}})} \tag{100}$$

$$\begin{cases} C_{45} = C_{47} = \dfrac{C_{39}\Delta_4\Delta_5}{\cos\beta\dfrac{L}{2}(e^{\frac{\alpha L}{2}} + e^{-\frac{\alpha L}{2}})\left[(e^{\frac{\alpha L}{3}} - e^{-\frac{\alpha L}{3}}) + 2\sin\beta\dfrac{L}{3}\right]} \\ C_{46} = -C_{48} = \dfrac{C_{39}\Delta_4\Delta_6}{\cos\beta\dfrac{L}{2}(e^{\frac{\alpha L}{2}} + e^{-\frac{\alpha L}{2}})\left[(e^{\frac{\alpha L}{3}} - e^{-\frac{\alpha L}{3}}) + 2\sin\beta\dfrac{L}{3}\right]} \end{cases} \tag{101}$$

where the expressions of $\Delta_1$~$\Delta_6$ are given in Appendix 3.

## Appendix C

$$\begin{aligned} \Delta_1 &= e^{\alpha L} - e^{-\alpha L} + \sin\beta L - \cos\beta\frac{L}{3}(e^{\alpha\frac{2L}{3}} - e^{-\alpha\frac{2L}{3}}) \\ &+ \cos\beta\frac{2L}{3}(e^{\alpha\frac{L}{3}} - e^{-\alpha\frac{L}{3}}) + \sin\beta\frac{L}{3}(e^{\alpha\frac{2L}{3}} + e^{-\alpha\frac{2L}{3}}) - \sin\beta\frac{2L}{3}(e^{\alpha\frac{L}{3}} + e^{-\alpha\frac{L}{3}}) \end{aligned} \tag{102}$$

$$\Delta_2 = \frac{C_{15}\left[\sin\beta\dfrac{L}{3}(e^{\frac{2}{3}\alpha L} - e^{-\frac{2}{3}\alpha L}) + \sin\beta\dfrac{2L}{3}(e^{\frac{\alpha L}{3}} - e^{-\frac{\alpha L}{3}})\right]}{\cos\beta\dfrac{L}{2}(e^{\frac{\alpha L}{2}} + e^{-\frac{\alpha L}{2}})\left[(e^{\frac{\alpha L}{3}} - e^{-\frac{\alpha L}{3}}) + 2\sin\beta\dfrac{L}{3}\right]} \tag{103}$$

$$\begin{aligned} \Delta_3 &= e^{\alpha L} - e^{-\alpha L} + \sin\beta L - \cos\beta(\frac{L}{2} - \frac{L_1}{2})(e^{\alpha(\frac{L}{2}+\frac{L_1}{2})} - e^{-\alpha(\frac{L}{2}+\frac{L_1}{2})}) + \\ &\cos\beta(\frac{L}{2} + \frac{L_1}{2})(e^{\alpha(\frac{L}{2}-\frac{L_1}{2})} - e^{-\alpha(\frac{L}{2}-\frac{L_1}{2})}) + \sin\beta(\frac{L}{2} - \frac{L_1}{2})(e^{\alpha(\frac{L}{2}+\frac{L_1}{2})} + e^{-\alpha(\frac{L}{2}+\frac{L_1}{2})}) \\ &- \sin\beta(\frac{L}{2} + \frac{L_1}{2})(e^{\alpha(\frac{L}{2}-\frac{L_1}{2})} + e^{-\alpha(\frac{L}{2}-\frac{L_1}{2})}) \end{aligned} \tag{104}$$

$$\Delta_4 = \sin\beta(\frac{L}{2} - \frac{L_1}{2})(e^{\alpha(\frac{L}{2}+\frac{L_1}{2})} - e^{-\alpha(\frac{L}{2}+\frac{L_1}{2})}) + \sin\beta(\frac{L}{2} + \frac{L_1}{2})(e^{\alpha(\frac{L}{2}-\frac{L_1}{2})} - e^{-\alpha(\frac{L}{2}-\frac{L_1}{2})}) \tag{105}$$

$$\Delta_5 = \cos\beta\frac{L_1}{2}(e^{\frac{\alpha L_1}{2}} - e^{-\frac{\alpha L_1}{2}}) - \sin\beta\frac{L_1}{2}(e^{\frac{\alpha L_1}{2}} + e^{-\frac{\alpha L_1}{2}}) \tag{106}$$

$$\Delta_6 = \cos\beta\frac{L_1}{2}(e^{\frac{\alpha L_1}{2}} - e^{-\frac{\alpha L_1}{2}}) + \sin\beta\frac{L_1}{2}(e^{\frac{\alpha L_1}{2}} + e^{-\frac{\alpha L_1}{2}}) \tag{107}$$